The Open Biomedical Engineering Journal
DOI: 10.2174/0118741207494787260915105045, 2026, 20, e18741207494787
ISSN: 1874-1207
1

RESEARCH ARTICLE **OPEN ACCESS**

Obesity Induced Intradiscal Stress Amplification Following Lumbar Foraminoplasty: Implications for Reherniation Risk

Iqbal Nur Arif[1,2], Denys Bungaran[1,2], Hasyid Ahmad Wicaksono[1,2], Tri Indah Winarni[2,3,4], Mohamad Izzur Maula[1,2], M. Danny Pratama Lamura[5] and J. Jamari[1,2,*]

[1]*Department of Mechanical Engineering, Faculty of Engineering, Diponegoro University, Tembalang, Semarang 50275, Central Java, Indonesia*
[2]*Undip Biomechanics Engineering & Research Centre (UBM-ERC), Diponegoro University, Tembalang, Semarang 50275, Central Java, Indonesia*
[3]*Department of Anatomy, Faculty of Medicine, Diponegoro University, Tembalang, Semarang 50275, Central Java, Indonesia*
[4]*Center for Biomedical Research (CEBIOR), Faculty of Medicine, Diponegoro University, Tembalang, Semarang 50275, Central Java, Indonesia*
[5]*Department of Mechanical Engineering, Faculty of Engineering and Science, Universitas Pembangunan Nasional Veteran Jawa Timur, Surabaya 60294, East Java, Indonesia*

Abstract:

Introduction/Objective: Recurrent lumbar disc herniation after endoscopic lumbar surgery remains a concern, particularly in patients with elevated body mass index (BMI). Although foraminoplasty relieves neural foraminal compression, partial facet resection may alter postoperative load transmission and intradiscal stress. This study assessed the biomechanical influence of BMI-derived axial loading on intradiscal stress distribution in the post-foraminoplasty L4–L5 segment and its potential implication for reherniation risk.

Methods: A three-dimensional L4–L5 finite element model was reconstructed from CT images of a healthy adult male. Foraminoplasty was simulated by partial resection of the L5 superior articular process. Five BMI-derived axial loads (394.65–794.98 N) were combined with 10 N·m moments during flexion, extension, lateral bending, and axial rotation. Maximum von Mises stress was evaluated separately in the annulus fibrosus and nucleus pulposus using descriptive quantitative comparisons.

Results: Nucleus pulposus stress generally increased with loading. During flexion, it rose from 0.4165 to 0.5843 MPa, representing a 40.29% increase, and flexion produced the highest nucleus pulposus stress under all loads. Annulus fibrosus stress also showed an overall load-dependent increase, although the motion producing the maximum value varied. During flexion, it increased from 1.9450 to 2.4420 MPa (25.55%). The overall maximum annulus fibrosus stress was 2.6613 MPa during left lateral bending at 794.98 N. Stress localized predominantly posteriorly in the nucleus pulposus and anterolaterally or posterolaterally in the annulus fibrosus.

Discussion: These compartment-specific responses indicate that postoperative disc mechanics are jointly influenced by axial load magnitude and motion direction, potentially increasing mechanical vulnerability under elevated loading.

Conclusion: BMI-related loading should be considered in surgical planning and postoperative rehabilitation to minimize unfavorable disc stress and potential reherniation risk after foraminoplasty.

Keywords: Finite element analysis, Lumbar spine, Foraminoplasty, Obesity, L4–L5, Spinal stress, Disc herniation, Reherniation risk.

© 2026 The Author(s). Published by Bentham Open.
This is an open access article distributed under the terms of the Creative Commons Attribution 4.0 International Public License (CC-BY 4.0), a copy of which is available at: https://creativecommons.org/licenses/by/4.0/legalcode. This license permits unrestricted use, distribution, and reproduction in any medium, provided the original author and source are credited.

*Address correspondence to this author at the Department of Mechanical Engineering, Faculty of Engineering, Diponegoro University, Tembalang, Semarang 50275, Central Java, Indonesia; Undip Biomechanics Engineering & Research Centre (UBM-ERC), Diponegoro University, Tembalang, Semarang 50275, Central Java, Indonesia;
E-mail: j.jamari@gmail.com

Cite as: Arif I, Bungaran D, Wicaksono H, Winarni T, Maula M, Lamura M, Jamari J. Obesity Induced Intradiscal Stress Amplification Following Lumbar Foraminoplasty: Implications for Reherniation Risk. Open Biomed Eng J, 2026; 20: e18741207494787. http://dx.doi.org/10.2174/0118741207494787260915105045

Received: April 20, 2026
Revised: July 20, 2026
Accepted: August 03, 2026
Published: October 29, 2026

Send Orders for Reprints to reprints@benthamscience.net

1. INTRODUCTION

The lumbar spine is a part of the human body that plays a vital role in supporting movement in daily life. Daily activities may be disrupted, and severe pain may be experienced due to diseases affecting the lumbar spine [1]. Herniated Nucleus Pulposus (HNP) is one of the common problems experienced by people. A condition in which the inner core of the disc (nucleus pulposus) protrudes through its outer layer (annulus) and pinches the nearby nerves; this condition is also typically accompanied by disc degeneration. In certain cases, a decrease in disc height due to degeneration may cause narrowing of the foraminal area and compress the nerves in that region, resulting in lower back pain. Percutaneous Transforaminal Endoscopic Discectomy (PTED) is a commonly used method for treating HNP. This procedure is performed *via* the Kambin triangle to remove the herniated tissue of the disc. Meanwhile, foraminoplasty is a key step in PTED and the method generally used to address narrowing of the foramen [2]. Although PTED has been proven effective in reducing pain in patients and has shown significant advancements in its endoscopic instruments, with surgical precision having improved, various risk still carried, such as the potential for instability in the spinal segment due to the bone intervention performed [3].

Compared to conventional open surgery and endoscopic nucleotomy, PTED has been associated with a higher and earlier rate of postoperative recurrence, which may adversely impact clinical outcomes [4]. Recurrence is reherniation at the same level and side following a pain-free interval after successful disc removal. It is classified as early (<6 months) or late (>6 months) [5, 6]. Meta-analytic data demonstrated that early and late recurrence rates were pooled at 2.1% and 1.2%, with peak cases reaching 2.9% for early and 1.9% for late recurrence, which, in early recurrence, represented nearly 61.7% of all reported recurrent incidences. Highlighting the necessity of close postoperative monitoring during the initial recovery phase [7]. Recurrence may happen even in the absence of clear risk factors, indicating that structural vulnerability within the disc space can persist despite surgical decompression [8].

Recent clinical evidence has further examined the relationship between body mass index and recurrent lumbar disc herniation following endoscopic lumbar surgery. A quantitative review of nine case-control studies involving 5,446 patients [9] found that patients who developed recurrent lumbar disc herniation after percutaneous endoscopic lumbar discectomy had a significantly higher BMI than those without recurrence, with a pooled weighted mean difference of 1.16 kg/m^2 (95% CI: 0.69–1.62) [9]. The same analysis identified older age, Modic changes, advanced disc degeneration, and a greater sacral slope as additional recurrence-associated factors [9]. More recently, a retrospective cohort study involving 1,278 patients identified elevated BMI as an independent predictor of early recurrence after percutaneous endoscopic lumbar discectomy [10]. These findings provide contemporary clinical support for considering excess body mass as a potential contributor to recurrent disc herniation after endoscopic decompression.

Nevertheless, the available clinical evidence is not entirely consistent. A systematic review and meta-analysis [11] comparing obese and non-obese patients undergoing full-endoscopic transforaminal discectomy found no statistically significant difference in recurrence rates, although obese patients had a higher overall postoperative complication rate (OR: 2.68; 95% CI: 1.21–5.93) [11]. Similarly, a retrospective cohort study reported comparable functional outcomes between obese and non-obese patients at 24 months following percutaneous transforaminal endoscopic surgery, with only one recurrent case observed in the obese group [12]. These varying findings may reflect differences in surgical techniques, BMI classifications, sample sizes, follow-up durations, and definitions of recurrence. Importantly, although clinical studies can identify associations between elevated BMI and postoperative recurrence, they do not directly explain how increased body-mass-related loading alters the mechanical environment of the postoperative intervertebral disc.

Against this clinical background, finite element analysis provides a controlled approach for examining postoperative spinal mechanics that cannot be directly isolated through clinical observations alone [13]. Previous finite element studies of PTED and foraminoplasty have primarily investigated the effects of surgical geometry and tissue removal on lumbar stability. A finite element study evaluating foraminoplasty at different portions of the L5 superior facet reported changes in segmental range of motion and intradiscal pressure [14]. Another in-silico study comparing limited foraminoplasty with a procedure involving larger annuloplasty and nucleotomy demonstrated that the extent of facet, annular, and nuclear tissue removal influenced postoperative biomechanical responses [15]. A

further finite element analysis showed that more extensive superior articular process resection, particularly when involving the articular surface or isthmus, resulted in asymmetric stress redistribution and increased segmental instability [16].

More recently, a BMI-related finite element study incorporated increasing body-mass-related loading into a model of percutaneous endoscopic transforaminal discectomy and reported progressive increases in nucleus pulposus stress and deformation, particularly during flexion [17]. However, their surgical model incorporated combined resection of the superior articular process, posterior annulus fibrosus, and nucleus pulposus, while the primary disc-level analysis focused on nucleus pulposus stress and deformation. Consequently, the magnitude and regional localization of stress in both the annulus fibrosus and nucleus pulposus within a defined post-foraminoplasty geometry remain insufficiently characterized [16].

CT-based subject-specific finite element modeling has increasingly been used to preserve individual spinal geometry while evaluating biomechanical responses under controlled loading conditions. A subject-specific lumbar finite element study developed and validated a functional spinal unit model and examined body-weight-related loading during flexion, extension, lateral bending, and axial rotation [18]. Recent patient-specific modeling workflows have also improved the reproducibility and scalability of CT-based lumbar finite element model generation [19]. A previous BMI-related finite element model [17] similarly demonstrated progressive increases in nucleus pulposus stress and deformation in normal and post-PETD lumbar models, particularly during flexion. However, these studies primarily focused on intact or discectomy-related models and evaluated the nucleus pulposus or overall disc response. The separate stress magnitude and regional localization of the annulus fibrosus and nucleus pulposus within a fixed post-foraminoplasty L4–L5 geometry remain insufficiently characterized.

Based on the expected load-dependent response of the intervertebral disc, we hypothesized that progressively greater BMI-derived axial compressive loads would result in higher von Mises stress in both the annulus fibrosus and nucleus pulposus. We further hypothesized that flexion would produce the greatest stress response and that elevated loading would accentuate stress concentration within mechanically vulnerable posterior and posterolateral disc regions.

2. MATERIALS AND METHODS

2.1. Geometric Parameters and Material Properties

The lumbar spine model was developed from computed tomography (CT) images of a 55-year-old Indonesian man. He had a body weight of 66 kg and a height of 168 cm. His bone condition was considered normal based on both clinical evaluation and radiological examination.

The CT scan data featured high-resolution images of the lumbar spine with a slice thickness of 1.0 mm. A single CT-derived anatomy was used because the objective of this study was to perform a controlled within-model comparison of BMI-derived axial loading rather than to estimate population-level variability. The same geometry, material properties, contact definitions, surgical configuration, and boundary conditions were maintained across all five loading scenarios. Consequently, differences in the predicted stress responses could be evaluated primarily as a function of axial load magnitude. Similar single-subject CT-based finite element approaches have been used for controlled comparative analyses of lumbar biomechanics [18, 20]. Data collection was performed with the volunteer's informed consent. The subject was recruited through the Department of Spinal Surgery at Dr. Kariadi General Hospital, Semarang, Indonesia. The study protocol was approved by the Ethical Committee of Medical Faculty, Diponegoro University, Semarang, Indonesia (Ethical Approval No. 108/EC/KEPK/FK-UNDIP/IV/2022). The study was conducted in accordance with the principles of the Declaration of Helsinki.

The imaging data were then processed using Mimics 21.0 (Materialise, Belgium) to segment the L4–L5 vertebrae and generate the initial three-dimensional geometry as the base model. The STL file derived from this initial geometry was subsequently refined and prepared for analysis in ANSYS Workbench 2023 R2 (Ansys, USA) prior to testing.

To distinguish between cortical and cancellous bone, each vertebral body was modeled as a cancellous core surrounded by a cortical shell. The cortical shell was generated along the outer vertebral surface with a variable thickness of 0.5–1.0 mm, while the remaining internal volume was assigned as cancellous bone. This modeling approach allowed the vertebrae to preserve the anatomical distinction between the stiffer outer cortical layer and the less dense internal cancellous region.

Maintaining consistency between the material assignment in a finite element model and the actual properties of spinal tissues is considered important for achieving a more reliable biomechanical representation. Accordingly, the material properties of the modeled spinal structures were assigned based on previously reported finite element parameters [21]. The material properties used for each spinal structure, including elastic modulus and Poisson's ratio, are presented in Table **1** to support model fidelity and to provide a consistent reference for future simulations.

To make the model biomechanically closer to the real spinal condition, seven ligament structures were also included: the anterior longitudinal ligament (ALL), posterior longitudinal ligament (PLL), interspinous ligament (ISL), supraspinous ligament (SSL), ligamentum flavum (LF), intertransverse ligament (ITL), and capsular ligament (CL). These ligaments were modeled as nonlinear spring elements with tension-only behavior, which follows their physiological role. Most of the ligament material properties were adopted from a previously published finite element model [21]. A complete summary of the modeling parameters is provided in Table **2**.

Table 1. Material properties were defined for each spinal component in the FEA model.

Component	Element Type	Young Modulus (MPa)	Poisson's ratio
Cortical Bone	Isotropic, Tetra element	12000	0.3
Annulus Fibrosus	Isotropic, Tetra element	4.2	0.45
Endplate	Isotropic, Tetra element	2000	0.2
Nucleus Pulposus	Isotropic, Tetra element	1	0.5
Cancellous	Isotropic, Tetra element	100	0.2

Table 2. Material properties for various ligament components in the FEA model.

Ligament	Element Type	Mechanical Behavior	Young Modulus (MPa)	Poisson's ratio
ALL	Spring elements	Tension-only	7.8	0.3
PLL	Spring elements	Tension-only	10	0.3
CL	Spring elements	Tension-only	8	0.3
LF	Spring elements	Tension-only	8	0.3
SSL	Spring elements	Tension-only	10	0.3
ISL	Spring elements	Tension-only	7.8	0.3
ITL	Spring elements	Tension-only	8	0.3

2.2. Model PTED Foraminoplasty

The finite element model was developed and focused on a single functional spinal unit (FSU), the L4–L5 segment. This segment was chosen because it is one of the lumbar levels most often involved in disc herniation and stenosis, making it highly relevant from a clinical perspective. The postoperative geometry of the L4–L5 FSU was reconstructed from anatomical references. The goal was to create a post-foraminoplasty model that could approximate the actual postoperative condition more closely. A defined resection was also made at the apex of the L5 superior articular process (SAP). This was intended to represent extensive decompression, a procedure often required when the neural foramen is severely narrowed.

The resection configuration used in this study was determined with reference to a previously published finite element framework [16] which categorized foraminoplasty resections into five groups (A–E). Group A served as the intact model. Group B involved ventral resection of the superior articular process without exposing the articular surface. Group C, the apex resection group, included excision of the SAP apex with partial exposure of the articular surface and removal of the adjacent capsular ligament. Groups D and E involved progressively more extensive resections, incorporating removal of the isthmus and lateral recess, and in Group D, even part of the L5 pedicle notch.

Based on previous findings, Group B resections produced negligible changes in intervertebral disc stress and range of motion (ROM), rendering them unsuitable for evaluating stress redistribution. Conversely, Groups D and E induced substantial increases in intervertebral disc stress (IDS) and kinematic instability, making them less clinically representative and potentially unsuitable for stable finite element simulations. Group C was therefore selected for the present study, as it represents a biomechanical threshold in which the facet joint is partially compromised, allowing for meaningful stress redistribution without introducing excessive instability. This configuration also reflects a clinically realistic decompression extent frequently performed during moderate foraminoplasty. The geometric characteristics of the adopted resection, including articular surface exposure, are illustrated in Fig. (**1**).

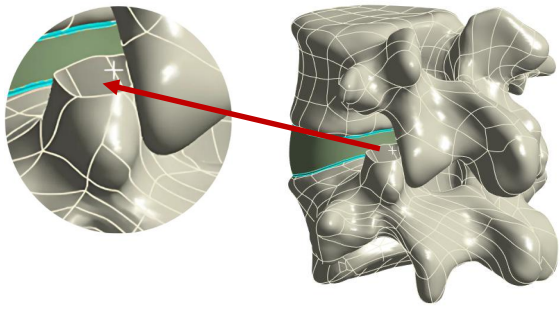

Fig. (1). Group C (apex resection) foraminoplasty model. The apex of the left L5 superior articular process (SAP) was resected with partial exposure of the articular surface.

2.3. Boundary Condition

To replicate physiological loading conditions of the lumbar spine, the finite element model of the L4–L5 segment was subjected to a compressive force of 500 N to simulate the upper body load, combined with an applied moment of 10 N·m to induce representative spinal motions, including flexion, extension, lateral bending, and axial rotation [21]. The compressive load was applied to the superior surface of the L4 vertebra, while the inferior surface of the L5 vertebra was fixed in all degrees of freedom to provide a stable boundary condition. The applied moment was imposed on the superior region of L4

according to the corresponding direction of each simulated motion. These loading scenarios reflect typical biomechanical demands experienced during routine activities of daily living. The resulting segmental ROM and von Mises stress distribution within the intervertebral disc were computed to evaluate the mechanical behavior of the spinal segment.

To enhance physiological relevance, the boundary conditions were further adapted using BMI-derived axial compressive loading scenarios. The compressive loads were scaled using factors derived from the estimated body mass of each BMI category relative to the normal-weight condition. Accordingly, the applied axial loads were 394.65 N, 500 N, 615.89 N, 665.93 N, and 794.98 N, representing underweight, normal weight, at-risk of obesity, obesity Class I, and obesity Class II conditions, respectively [22]. The boundary conditions and anatomical configuration of the lumbar segment are illustrated in Fig. (**2**).

2.3.1. BMI-Derived Axial Loading Scenarios

The actual CT-based subject had a body mass of 66 kg and a height of 1.68 m. Using the standard BMI formula, BMI = body mass / height^2, the actual BMI of the subject was 23.38 kg/m^2. This value falls within the at-risk of obesity category and was used as the anchor BMI because it represents the actual subject used for finite element model reconstruction.

To generate BMI-based loading scenarios while maintaining the same spinal geometry, representative BMI values for the other categories were derived from this anchor BMI using the width of the Asia-Pacific BMI classification ranges. The normal-weight representative BMI was obtained by subtracting the width of the normal BMI range, 22.9–18.5, from the anchor BMI. The obesity Class I representative BMI was obtained by adding the width of the at-risk BMI range, 24.9–23.0, to the anchor BMI. The obesity Class II representative BMI was then obtained by adding the width of the obesity Class I range, 29.9–25.0. Because the underweight category has no defined lower bound, an operational width of 4.00 kg/m^2 was applied below the normal-weight representative BMI to define a conservative underweight loading scenario while avoiding an excessively low body-mass condition.

Because the same CT-based geometry was used for all simulations, the subject height was kept constant at 1.68 m. Each representative BMI value was then converted into estimated body mass using the BMI formula. The normal-weight condition was used as the reference condition and assigned an axial compressive load of 500 N. A scaling factor was then calculated for each BMI category by dividing the estimated body mass of that category by the estimated body mass of the normal-weight category. The axial load for each BMI category was obtained by multiplying the scaling factor by the reference load of 500 N.

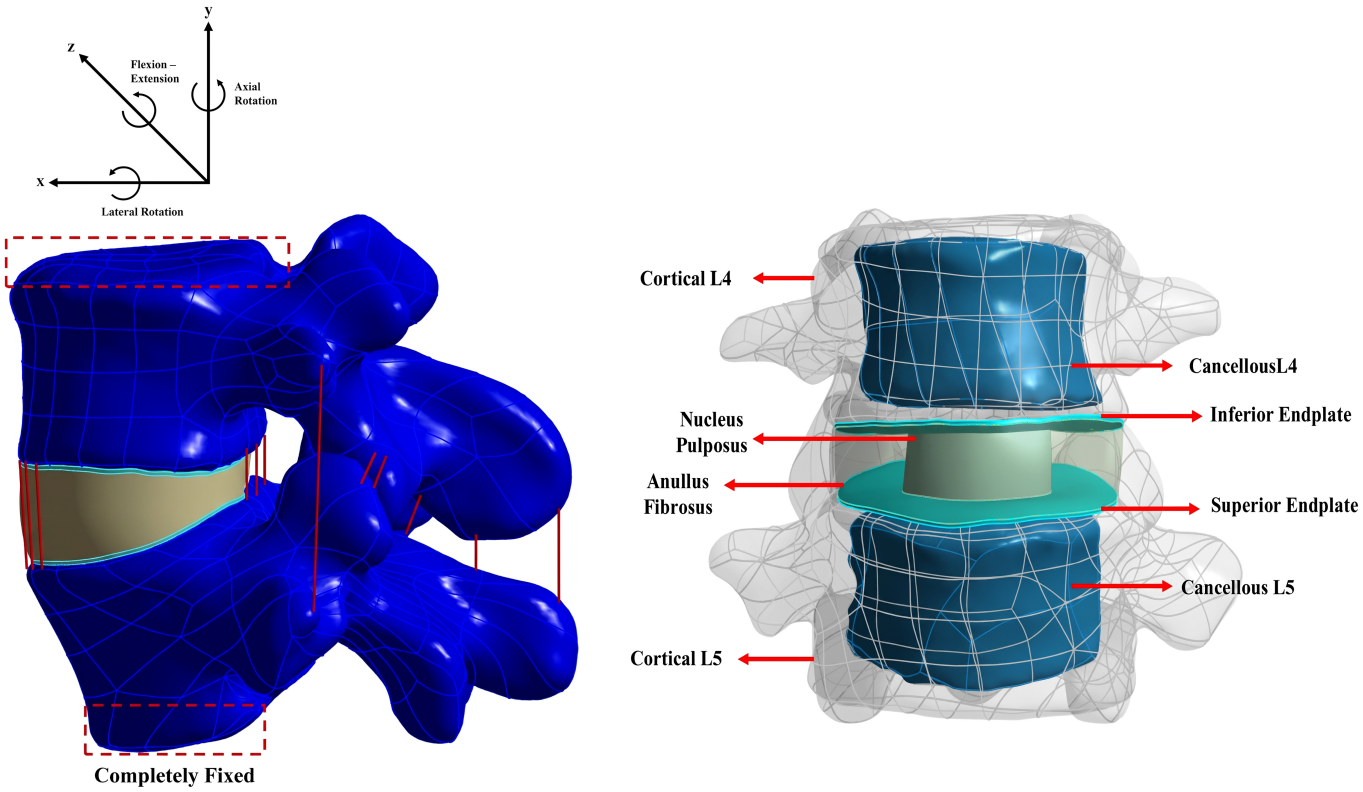

Fig. (2). The reconstructed model of the L4–L5 lumbar vertebrae.

BMI was represented through scaled axial compressive loading to isolate the mechanical effect of increasing body mass while maintaining the same model geometry, material properties, contact definitions, and boundary conditions. Obesity-related changes in posture, sagittal alignment, and muscle forces were not incorporated because they require additional subject-specific data and coupled musculoskeletal modeling. Therefore, the simulations should be interpreted as controlled BMI-derived loading scenarios rather than comprehensive representations of obesity-related spinal biomechanics. The resulting representative BMI values, estimated body masses, scaling factors, and applied axial loads are summarized in Table **3**.

2.4. Mesh Study

The solid components of the L4–L5 finite element model were discretized using ten-node quadratic tetrahedral elements. Mesh convergence was evaluated by progressively refining the element size and monitoring both maximum von Mises stress in the annulus fibrosus and total deformation. Maximum annulus fibrosus stress was selected as the principal convergence parameter because intradiscal stress was the primary outcome of the present study, whereas total deformation was used to evaluate the stability of the global structural response.

The predicted maximum annulus fibrosus stress varied at coarser element sizes but stabilized after the element size reached 1.0 mm. The maximum stress values obtained at element sizes of 1.0, 0.9, and 0.8 mm were 1.812, 1.800, and 1.810 MPa, respectively. The successive differences were approximately 0.66% between 1.0 and 0.9 mm and 0.56% between 0.9 and 0.8 mm. These differences were below the predefined convergence criterion of 1%, indicating that further mesh refinement produced only negligible changes in the predicted annulus fibrosus stress.

Total deformation was also assessed as a secondary convergence parameter. At an element size of 1.0 mm, the complete L4–L5 model contained 588,628 elements. Refinement to 0.9 mm increased the total number of elements to 800,803, representing an increase of approximately 36%, while the resulting total deformation differed by only 0.2%. Therefore, the 1.0-mm mesh was adopted for the subsequent simulations because both the local annulus fibrosus stress and global deformation responses had stabilized, while further refinement substantially increased the computational cost. The convergence behavior of the finite element model across different element sizes is illustrated in Fig. (**3**).

2.5. Validation Method

The finite element model was validated by comparing the predicted range of motion (ROM) of the L4–L5 segment with previously reported in vitro experimental data [23]. The simulations were performed under flexion–extension, lateral bending, and axial rotation loading conditions. To improve the physiological relevance of the model, the boundary conditions and external loading configuration were adopted from a previously published finite element method [21]. These loading and constraint conditions were used for model implementation and were not treated as a separate quantitative validation dataset.

Quantitative agreement was assessed using the absolute deviation and percentage deviation between the predicted ROM and the corresponding experimental mean. The absolute deviations were also expressed relative to the reported experimental standard deviations to account for inter-specimen variability. In addition, each predicted value was evaluated against the corresponding experimental mean ± standard deviation interval. The mean absolute error (MAE) across the three loading directions was calculated as an overall measure of prediction error. Because the present study employed a deterministic, single-geometry finite element model with one numerical prediction for each motion condition, the statistical assessment was descriptive rather than inferential; therefore, hypothesis testing and *p*-values were not applied.

The mean absolute error (MAE) was calculated to summarize the overall magnitude of the differences between the predicted and experimental mean ROM values across the three motion conditions:

$$MAE = \frac{1}{n}\sum_{i=1}^{n}|P_i - R_i|$$

where P_i represents the predicted ROM, R_i represents the corresponding experimental mean ROM, and $n$is the number of motion conditions evaluated (n = 3).

Table 3. BMI-derived axial loading scenarios used in the finite element analysis.

BMI Category	BMI Range	Representative BMI (kg/m^2)	Estimated Body Mass (kg)	Scaling Factor	Applied Axial Load (N)
Underweight	<18.5	14.98	42.29	0.78	394.65
Normal weight	18.5–22.9	18.98	53.58	1	500
At risk of obesity	23.0–24.9	23.38	66	1.23	615.89
Obesity Class I	25.0–29.9	25.28	71.36	1.33	665.93
Obesity Class II	≥30.0	30.18	85.19	1.59	794.98

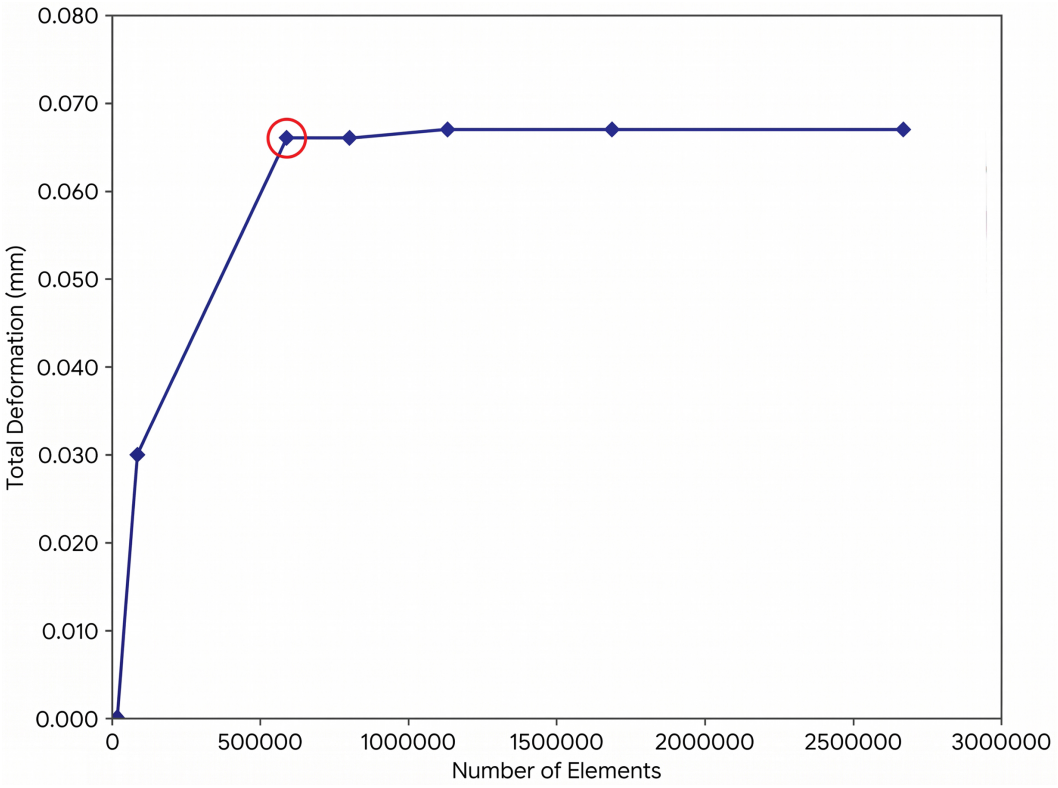

Fig. (3). Graphic representation of Mesh convergence study.

2.6. Quantitative Comparison of Stress Responses

Maximum von Mises stress was compared descriptively across the five BMI-derived axial loading scenarios for each motion direction and disc component. The 394.65 N condition was used as the reference. Absolute stress differences were calculated by subtracting the reference stress from the stress under each higher loading condition, while percentage changes were calculated relative to the reference value. Because the analysis was based on a deterministic single-geometry finite element model with one numerical output for each condition, inferential statistical tests and *p*-values were not applied.

3. RESULTS

3.1. Model Validation

The quantitative validation results are presented in Fig. (**4**) and Table **4**. The predicted ROM values were 14.70° for flexion–extension, 10.20° for lateral bending, and 2.50° for axial rotation. Compared with the reference experimental mean values [23], the corresponding absolute deviations were 0.10°, 2.00°, and 1.20°, representing percentage deviations of 0.68%, 16.39%, and 32.43%, respectively. The overall MAE across the three motion conditions was 1.10°.

Despite the differences relative to the experimental means, all predicted ROM values remained within the corresponding experimental mean ± standard deviation intervals. The predicted flexion–extension value was within the experimental interval of 12.70–16.90°, lateral bending was within 9.95–14.45°, and axial rotation was within 2.20–5.20°. When the absolute differences were expressed relative to the corresponding experimental standard deviations, the deviations were 0.05, 0.89, and 0.80 standard deviations for flexion–extension, lateral bending, and axial rotation, respectively.

Table 4. The intervertebral ROM results were compared to those reported in earlier studies for model validation.

Moment	Range of Motion (degree)		Absolute Deviation (°)	Percentage Deviation (%)	Deviation Relative to SD
	Present Study	Experimental Reference			
Flexion-extension	14.7	14.8 ± 2.10	0.10	0.68	0.05
Lateral bending	10.2	12.2 ± 2.25	2.00	16.39	0.89
Axial rotation	2.5	3.7 ± 1.50	1.20	32.43	0.80

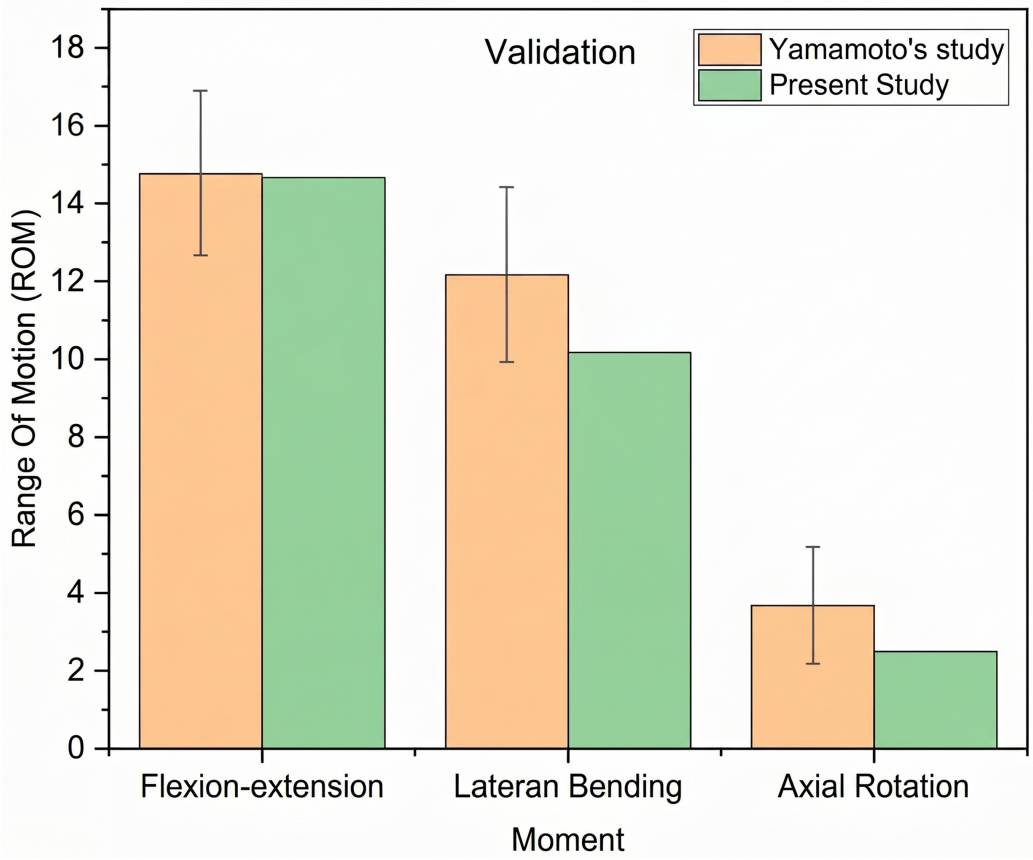

Fig. (4). Comparison of the predicted intervertebral ROM with the experimental reference data [23] used for model validation.

Axial rotation exhibited the highest percentage deviation. However, this result should be interpreted in conjunction with the absolute deviation and experimental variability. Because the experimental mean ROM for axial rotation was relatively small, an absolute difference of 1.20° produced a comparatively large percentage deviation. Nevertheless, the predicted axial-rotation value remained within one experimental standard deviation of the reference mean. The remaining discrepancies may be associated with subject-specific anatomical characteristics, differences in vertebral and facet geometry, the use of simplified isotropic linear-elastic material properties, the representation of ligaments using spring elements, variations in contact definitions, differences in boundary and loading conditions, and the inherent inter-specimen variability of experimental spinal measurements. Overall, the agreement with the experimentally reported ROM ranges supports the use of the model for the subsequent comparative biomechanical analyses.

3.2. Von Mises Stress on Vertebral Disk L4-L5

As shown in Fig. (**5**), maximum von Mises stress in the nucleus pulposus generally increased with greater BMI-derived axial compressive loading. Flexion consistently produced the highest nucleus pulposus stress across all five loading conditions, increasing from 0.41650 MPa at 394.65 N to 0.58430 MPa at 794.98 N. This corresponded to an absolute increase of 0.16780 MPa and a relative increase of 40.29%.

From the 394.65-N to the 794.98-N condition, nucleus pulposus stress increased by 246.61% during extension, 80.90% during left lateral bending, 90.08% during right lateral bending, 42.37% during left axial rotation, and 81.81% during right axial rotation. The large percentage increase during extension should be interpreted together with its low reference stress of 0.07771 MPa; the corresponding absolute increase was 0.19164 MPa, and the final extension stress remained lower than the flexion stress.

The response was not strictly monotonic at every adjacent loading step. A small decrease occurred during left axial rotation between 394.65 and 500 N and during right lateral bending between 615.89 and 665.93 N. Therefore, the results indicate an overall load-dependent increase rather than a uniformly progressive increase under every condition.

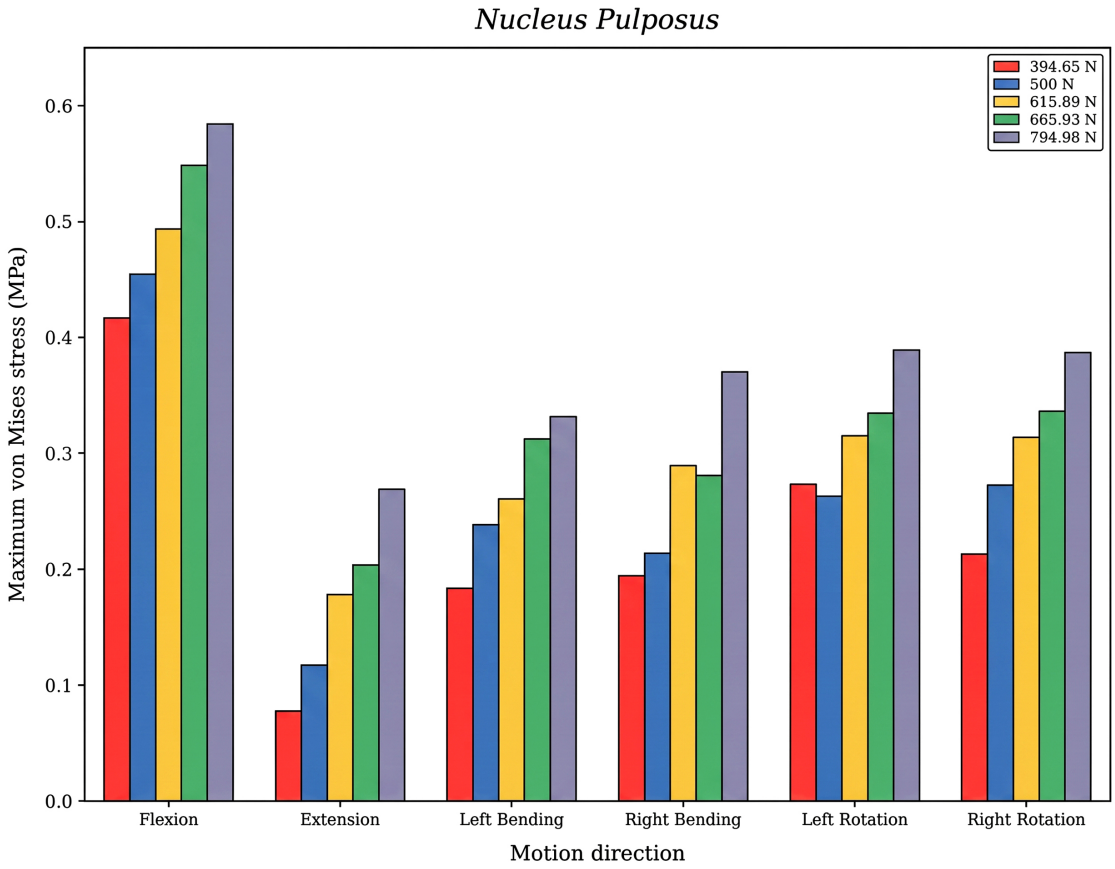

Fig. (5). Maximum von Mises stress in the nucleus pulposus under five BMI-derived axial loading conditions. Flexion produced the highest stress across all loading conditions, while the overall response generally increased with greater axial loading.

As shown in Fig. (**6**), maximum von Mises stress in the annulus fibrosus also demonstrated an overall increase with greater BMI-derived axial loading, although the response was not strictly monotonic and the motion producing the maximum stress varied among loading levels. During flexion, annulus fibrosus stress increased from 1.94500 MPa at 394.65 N to 2.44200 MPa at 794.98 N, corresponding to an absolute increase of 0.49700 MPa and a relative increase of 25.55%.

From the 394.65 N to the 794.98 N condition, annulus fibrosus stress increased by 21.99% during extension, 41.28% during left lateral bending, 17.26% during right lateral bending, 33.03% during left axial rotation, and 49.61% during right axial rotation. The overall maximum annulus fibrosus stress was 2.66130 MPa during left lateral bending at 794.98 N.

The dominant motion varied according to loading level. Right lateral bending produced the highest annulus fibrosus stress at 394.65 N, flexion at 500 and 615.89 N, right lateral bending at 665.93 N, and left lateral bending at 794.98 N. These findings indicate that annulus fibrosus stress was influenced by both axial load magnitude and motion direction.

Across the evaluated conditions, the magnitude and motion producing peak stress differed between the nucleus pulposus and annulus fibrosus.

3.3. Regional Stress Distribution

The stress contours in Fig. (**7**) showed that nucleus pulposus stress during flexion was predominantly concentrated in the posterior region. Across the evaluated loading conditions, the principal stress concentration remained generally posterior, although its magnitude varied with axial load.

Figure **8** showed two principal stress-concentration regions in the annulus fibrosus, located in the anterolateral and posterolateral regions. The relative prominence of these regions varied according to motion direction and axial loading condition.

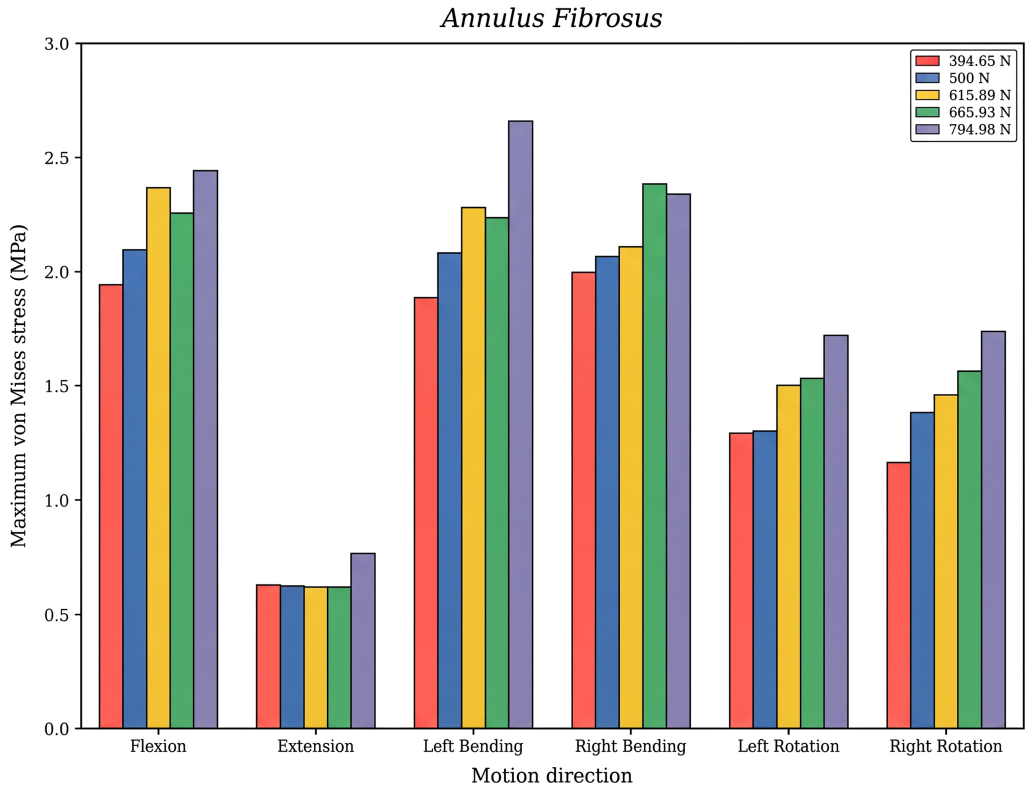

Fig. (6). Maximum von Mises stress in the annulus fibrosus under five BMI-derived axial loading conditions. The dominant motion varied among loading levels, and the overall maximum stress was 2.66130 MPa during left lateral bending at 794.98 N.

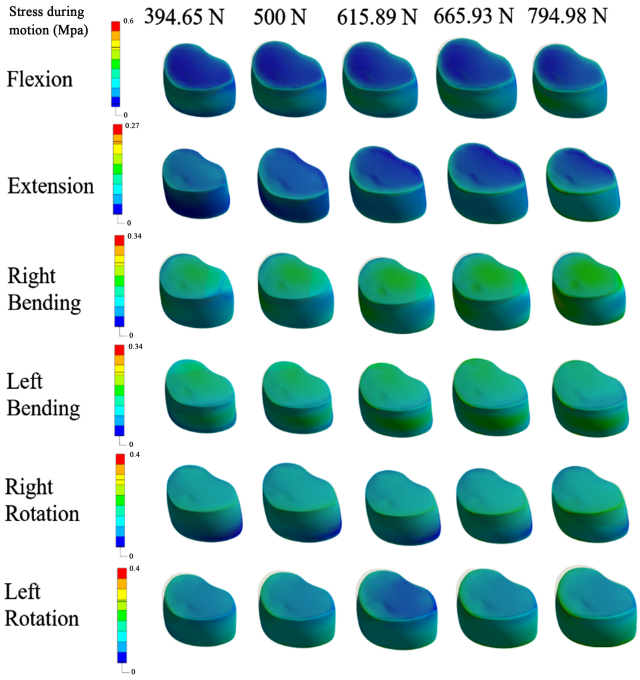

Fig. (7). Von Mises stress distribution in the nucleus pulposus under different motion and BMI-derived axial loading conditions. During flexion, stress was predominantly concentrated in the posterior region.

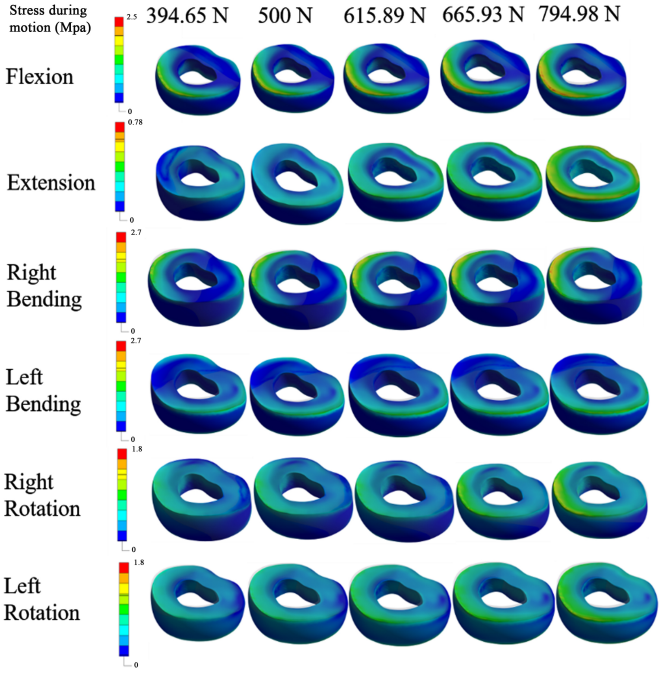

Fig. (8). Von Mises stress distribution in the annulus fibrosus under different motion and BMI-derived axial loading conditions. The principal stress concentrations were located in the anterolateral and posterolateral regions.

4. DISCUSSION

4.1. Influence of Axial Load Magnitude and Motion Direction

Overall, greater BMI-derived axial loading increased mechanical demand on both disc components, but the nucleus pulposus and annulus fibrosus exhibited different motion-dependent responses. The hypothesis was therefore partially supported: stress generally increased in both tissues and flexion consistently produced the highest nucleus pulposus stress, whereas the maximum annulus fibrosus stress varied among motion directions.

The simulations showed that increasing BMI-derived axial loading generally increased intradiscal stress, although the magnitude of the response differed among motion directions and was not uniform at every loading increment. Between 394.65 and 794.98 N, nucleus pulposus stress increased by 40.29–246.61%, whereas annulus fibrosus stress increased by 17.26–49.61%. Several small decreases occurred between adjacent loading conditions, but these variations did not alter the overall pattern of greater stress under the highest axial load.

The largest relative increase in nucleus pulposus stress occurred during extension, rising from 0.07771 to 0.26935 MPa. This percentage was amplified by the low initial value and therefore did not indicate that extension produced the greatest absolute mechanical demand. Flexion consistently generated the highest nucleus pulposus stress, reaching 0.58430 MPa at 794.98 N. In the annulus fibrosus, the motion associated with the maximum stress changed with loading level, and the highest value of 2.66130 MPa occurred during left lateral bending at 794.98 N. These results show that axial load magnitude and motion direction jointly determined the stress response of the two disc components.

Because an intact control model was not included, the present analysis cannot isolate the biomechanical effect of facet resection itself. The findings instead characterize load- and motion-dependent stress responses within the fixed post-foraminoplasty geometry.

4.2. Comparison with Previous Finite Element Studies

The present findings showed both agreement and differences with previous finite element studies. A previous BMI-related finite element study [17] reported that increasing BMI-related loading increased nucleus pulposus stress and deformation after PETD, with flexion producing the most pronounced response. This agrees with the present finding that flexion consistently generated the highest absolute nucleus pulposus stress. Previous foraminoplasty finite element models [16, 24] also demonstrated asymmetric and motion-dependent changes in surgical-level disc stress following superior articular process resection. However, in the present model, the motion producing the maximum annulus fibrosus stress varied across loading levels rather than remaining dominated by one motion direction. These differences may be related to variations in resection geometry, the inclusion or exclusion of annular and nuclear tissue removal, model extent, material definitions, and loading conditions.

Greater compressive loading can alter the mechanical environment of the lumbar segment and increase the demand placed on the intervertebral disc. Previous biomechanical studies have similarly shown that changes in physiological loading influence stress and strain within lumbar structures and affect the mechanical response of the annulus fibrosus [25, 26]. In the present post-foraminoplasty model, the nucleus pulposus was most sensitive during flexion, whereas annular stress showed a stronger dependence on motion direction.

Together, these comparisons indicate agreement in the load-dependent nucleus pulposus response while highlighting model-specific differences in the motion associated with peak annulus fibrosus stress.

4.3. Mechanical Significance of Regional Stress Distribution

The posterior concentration observed in the nucleus pulposus during flexion and the anterolateral and posterolateral concentrations in the annulus fibrosus are mechanically relevant because these regions are commonly associated with disc herniation in experimental and clinical literature [27-29]. In the present model, however, the contours identify regions of elevated stress rather than direct evidence of tissue damage or recurrent herniation.

Based on (Fig. **7**), the local stress concentration under flexion loading was predominantly distributed in the posterior region of the nucleus pulposus. This finding may initially appear counterintuitive, as flexion involves forward bending of the spine and the highest von Mises stress was observed during this movement. However, this phenomenon can be explained by the mechanical behavior of the intervertebral disc during flexion, in which compressive stress develops in the anterior annulus while tensile and shear stresses occur in the posterior region. This posterior stress concentration indicates backward migration of the nucleus pulposus during flexion, which increases the loading on the posterior annulus fibrosus. These observations are consistent with previous studies reporting that flexion induces posterior displacement of the nucleus and stress concentration in the posterior annulus, corresponding to the common site of disc herniation [30].

Based on (Fig. **8**), the von Mises stress distribution in the annulus fibrosus exhibited two principal concentration areas in the anterolateral and posterolateral regions. This pattern differed from the predominantly posterior concentration observed in the nucleus pulposus during flexion. The broader annular distribution is consistent with load transfer through the circumferential and radial structure of the annulus, while the relative prominence of each region varied with motion direction and axial loading. The posterolateral concentration therefore indicates locally elevated mechanical demand but does not establish annular failure or recurrent herniation.

The maximum annulus fibrosus von Mises stress obtained in the present study was 2.66130 MPa. Experimental tensile testing has reported estimated in situ vertical strengths of approximately 3.9 MPa for the anterior annulus and 8.6 MPa for the posterior annulus [31]. Thus, the maximum stress obtained in the present simulations was numerically below these reported experimental strengths.

Direct equivalence cannot be established because the experimental values represent direction-specific tensile strength, whereas the present study evaluated equivalent von Mises stress using an isotropic linear-elastic annulus model. Annulus fibrosus failure is anisotropic and multiaxial and is strongly influenced by fiber orientation and loading direction [32]. A formal safety factor was therefore not calculated. The reported stress values indicate increased mechanical demand but do not independently demonstrate annular damage or disc failure

4.4. Clinical Implications

The observed load-dependent stress response provides a mechanical context for clinical studies that have associated elevated BMI with less favorable outcomes or recurrent herniation after lumbar surgery [33-35]. The findings support considering body mass together with postoperative movement and loading conditions, while the present simulations do not directly demonstrate annular failure, nucleus extrusion, or recurrent herniation.

The lower equivalent stress observed during extension provides biomechanical context for postoperative movement planning, but it does not establish extension as universally safe or justify a single rehabilitation strategy [36–39]. Rehabilitation should remain individualized and may incorporate core stabilization and proprioceptive training according to symptoms, surgical extent, functional capacity, occupation, and other patient-specific factors [40].

4.5. Study Limitations

This study has several limitations. First, obesity was represented solely through BMI-derived axial compressive loading, while the underlying geometry, material properties, contact definitions, and applied moments were held constant. This controlled approach enabled the load-related mechanical effect of increasing body mass to be isolated; however, it did not capture other obesity-associated biomechanical factors, including altered sagittal alignment, posture, muscle recruitment, muscle-generated forces, fat distribution, and tissue quality. In addition, the simulations were limited to axial compression combined with pure moments and therefore did not reproduce dynamic loading, combined multiplanar movements, or the full complexity of physiological spinal loading. Accordingly, the findings should be interpreted as comparative axial-loading responses within a fixed post-foraminoplasty geometry rather than as comprehensive patient-specific simulations of obesity-related spinal biomechanics.

Second, the study evaluated a single post-foraminoplasty L4–L5 geometry without an intact control model. A single CT-derived anatomy was intentionally used to maintain the same anatomical geometry, material properties, contact definitions, surgical configuration, and boundary conditions across all BMI-derived loading scenarios, thereby allowing the mechanical effect of axial load magnitude to be evaluated under controlled conditions. Similar subject-specific CT-based finite element approaches have been used in previous lumbar biomechanical studies [18, 20]. However, the use of a single anatomy does not capture inter-individual variations in disc dimensions, facet orientation, vertebral morphology, sagittal alignment, and local tissue properties, which may influence both the magnitude and location of peak stress. In addition, because an intact control model was not included, the present analysis cannot independently quantify the biomechanical effect of foraminoplasty relative to the intact lumbar segment. Therefore, the findings are most applicable to the direction and relative pattern of the load-dependent response within the reconstructed anatomy rather than to population-wide absolute stress values. Future studies should repeat the loading protocol across multiple CT-derived geometries and include an intact control model to determine the robustness of the observed patterns.

Third, the surgical model did not incorporate several discectomy-related changes, including annulus fibrosus defects, reduction in nucleus pulposus volume, endplate injury, or other procedure-associated tissue alterations. Several surgical steps were also not explicitly simulated. Consequently, the model represents a simplified post-foraminoplasty condition rather than the complete anatomical changes produced by PTED. No anisotropic tissue-damage or failure criterion was assigned to the annulus fibrosus; therefore, the model could not determine the onset of fiber damage, delamination, or rupture.

Fourth, the finite element model did not incorporate the biomechanical effects of neural decompression. Although nerve decompression is clinically important, its influence on postoperative movement and patient behavior cannot be directly represented using the present structural model. The remaining differences from experimental ROM may also reflect subject-specific geometry, simplified isotropic material behavior, ligament representation, contact definitions, and inter-specimen variability. Future studies should combine multiple subject-specific postoperative anatomies, muscle loading, sagittal alignment, an intact control model, and more comprehensive surgical and damage formulations to improve the physiological relevance of the simulations.

CONCLUSION

This finite element study showed that greater BMI-derived axial compressive loading generally increased maximum von Mises stress in both the nucleus pulposus and annulus fibrosus within a fixed post-foraminoplasty L4–L5 geometry. Flexion consistently produced the highest nucleus pulposus stress, whereas the motion producing the maximum annulus fibrosus stress varied with loading level.

The stress contours identified posterior concentration in the nucleus pulposus and anterolateral and posterolateral concentrations in the annulus fibrosus. These patterns indicate regions of elevated mechanical demand, but the reported values do not directly demonstrate tissue failure or recurrent herniation.

The findings support considering body-mass-related loading and motion direction together in biomechanical assessment and future postoperative planning. Confirmation across multiple anatomies, more complete surgical models, and anisotropic damage-based material formulations is required.

AUTHORS' CONTRIBUTIONS

The authors confirm their contributions to the paper as follows: I.N.A: Study Conception and Design, Analysis and interpretation, First drafting and revision manuscript; D.B.: Data collection, Analysis and interpretation of results, and revision manuscript; H.A.W.: Data collection, Analysis and interpretation of results, and revision manuscript; T.I.W.: Study conception and design, Analysis and interpretation of results, supervising, and revision manuscript, M.I.M.: Data collection, Analysis and interpretation of results, revision manuscript; M.D.P.L.: Study conception and design, and revision manuscript; J.J.: Study conception and design, Analysis and interpretation of results, supervising, revision manuscript. All authors reviewed the results and approved the final version of the manuscript.

LIST OF ABBREVIATIONS

BMI	=	Body Mass Index
FEA	=	Finite Element Analysis
FSU	=	Functional Spinal Unit
HNP	=	Herniated Nucleus Pulposus
PTED	=	Percutaneous Transforaminal Endoscopic Discectomy
ROM	=	Range of Motion
SAP	=	Superior Articular Process

ETHICS APPROVAL AND CONSENT TO PARTICIPATE

The study protocol was approved by the Ethical Committee of the Medical Faculty, Diponegoro University, Semarang, Indonesia (Ethical Approval No. 108/EC/KEPK/FK-UNDIP/IV/2022).

HUMAN AND ANIMAL RIGHTS

All procedures involving human participants were conducted in accordance with the ethical standards of the committee responsible for human experimentation (institutional and national), and with the Helsinki Declaration of 1975, as revised in 2013.

CONSENT FOR PUBLICATIONS

Informed consent was obtained from the volunteer prior to data collection and the use of the individual data for this study.

STANDARDS OF REPORTING

STROBE guidelines were followed.

AVAILABILITY OF DATA AND MATERIALS

The data supporting the findings of this study are available from the corresponding author, [J.J.], upon reasonable request.

FUNDING

This work was supported by the Riset Konsorsium Unggulan Berdampak (RIKUB) 2025 from the Ministry of Higher Education, Science, and Technology/Kementerian Pendidikan Tinggi, Sains, dan Teknologi (Kemdiktisaintek), Republic of Indonesia under contract no. 629-02/UN7.D2/PP/VIII/2025

CONFLICT OF INTEREST

The authors declare no conflict of interest, financial or otherwise.

ACKNOWLEDGEMENTS

The authors also appreciate the valuable contributions of all laboratory partners at the Undip Biomechanics Engineering and Research Centre (UBM-ERC), Indonesia to the experimental setup and data analysis

REFERENCES

[1] D. Hoy, L. March, P. Brooks, F. Blyth, A. Woolf, C. Bain, G. Williams, E. Smith, T. Vos, J. Barendregt, C. Murray, R. Burstein, and R. Buchbinder, "The global burden of low back pain: Estimates from the Global Burden of Disease 2010 study", *Ann. Rheum. Dis.*, vol. 73, no. 6, pp. 968-974, 2014. [http://dx.doi.org/10.1136/annrheumdis-2013-204428] [PMID: 24665116]

[2] A.A. Fanous, L.M. Tumialán, and M.Y. Wang, "Kambin's triangle: Definition and new classification schema", *J. Neurosurg. Spine*, vol. 32, no. 3, pp. 390-398, 2020. [http://dx.doi.org/10.3171/2019.8.SPINE181475] [PMID: 31783346]

[3] K. Jitpakdee, Y. Liu, D.H. Heo, V. Kotheeranurak, S. Suvithayasiri, and J. Kim, "Minimally invasive endoscopy in spine surgery: Where are we now?", *Eur. Spine J.*, vol. 32, no. 8, pp. 2755-2768, 2023. [http://dx.doi.org/10.1007/s00586-023-07622-7] [PMID: 36856868]

[4] Z. Chen, L. Zhang, J. Dong, P. Xie, B. Liu, Q. Wang, R. Chen, T. Shu, S. Li, F. Feng, B. Yang, L. He, Y. Yang, Z. Liu, M. Pang, and L. Rong, "Percutaneous transforaminal endoscopic discectomy versus microendoscopic discectomy for lumbar disc herniation", *Spine*, vol. 45, no. 8, pp. 493-503, 2020. [http://dx.doi.org/10.1097/BRS.0000000000003314] [PMID: 31703056]

[5] Y. Yao, H. Liu, H. Zhang, H. Wang, C. Zhang, Z. Zhang, J. Wu, Y. Tang, and Y. Zhou, "Risk factors for recurrent herniation after percutaneous endoscopic lumbar discectomy", *World Neurosurg.*, vol. 100, pp. 1-6, 2017. [http://dx.doi.org/10.1016/j.wneu.2016.12.089] [PMID: 28043884]

[6] H.S. Kim, and J.Y. Park, "Comparative assessment of different percutaneous endoscopic interlaminar lumbar discectomy (PEID) techniques", *Pain Physician*, vol. 16, no. 4, pp. 359-367, 2013. [http://dx.doi.org/10.36076/ppj.2013/16/359] [PMID: 23877452]

[7] S. Yin, H. Du, W. Yang, C. Duan, C. Feng, and H. Tao, "Prevalence of recurrent herniation following percutaneous endoscopic lumbar discectomy: A meta-analysis", Pain Physician, vol. 21, no. 4, pp.

337-350, 2018.
[http://dx.doi.org/10.36076/ppj.2018.4.337] [PMID: 30045591]

[8] L.Y. Dai, Q. Zhou, W.F. Yao, and L. Shen, "Recurrent lumbar disc herniation after discectomy: Outcome of repeat discectomy", *Surg. Neurol.,* vol. 64, no. 3, pp. 226-231, 2005.
[http://dx.doi.org/10.1016/j.surneu.2004.11.003] [PMID: 16099250]

[9] J. Zhao, L. Zeng, S. Zhao, G. Liang, B. Sha, H. Fu, W. Yang, J. Liu, and Y. Zeng, "Associations of recurrent lumbar disc herniation after percutaneous endoscopic lumbar discectomy with age, body mass index, modic change, disc degeneration and sacral slope: A quantitative review", *Exp. Ther. Med.,* vol. 27, no. 5, p. 195, 2024.
[http://dx.doi.org/10.3892/etm.2024.12483] [PMID: 38544559]

[10] S. Thongpech, V. Kuansongtham, S. Neti, T. Wattanawong, W. Kesornsak, P. Kasempipatchai, K.M.M. Lwin, B. Sakboonyarat, and K. Pongpirul, "Early recurrence of herniated nucleus pulposus after percutaneous endoscopic lumbar discectomy: A retrospective cohort study of 1,278 patients", *Surg. Neurol. Int.,* vol. 16, p. 322, 2025.
[http://dx.doi.org/10.25259/SNI_574_2025] [PMID: 41030400]

[11] A.P. Feng, S.F. Yu, C.M. Chen, L.R. He, S.W. Jhang, and G.X. Lin, "Comparative outcomes of obese and non-obese patients with lumbar disc herniation receiving full endoscopic transforaminal discectomy: A systematic review and meta-analysis", *BMC Musculoskelet. Disord.,* vol. 25, no. 1, p. 322, 2024.
[http://dx.doi.org/10.1186/s12891-024-07455-5] [PMID: 38654321]

[12] C. Zhuang, Y. Xu, H. Lin, and Y. Gu, "The influence of body mass index on efficacy and outcomes of percutaneous transforaminal endoscopic surgery (PTES) for the treatment of lumbar degenerative diseases: A retrospective cohort study", *BMC Surg.,* vol. 25, no. 1, p. 28, 2025.
[http://dx.doi.org/10.1186/s12893-025-02761-8] [PMID: 39819484]

[13] M.C. Wang, A. Kiapour, E. Massaad, J.H. Shin, and N. Yoganandan, "A guide to finite element analysis models of the spine for clinicians", *J. Neurosurg. Spine,* vol. 40, no. 1, pp. 38-44, 2024.
[http://dx.doi.org/10.3171/2023.7.SPINE23164] [PMID: 37856396]

[14] Y. Yu, Q. Zhou, Y. Xie, X. Wang, X. Fan, D. Gu, X. Huang, and W. Wu, "Effect of percutaneous endoscopic lumbar foraminoplasty of different facet joint portions on lumbar biomechanics: A finite element analysis", *Orthop. Surg.,* vol. 12, no. 4, pp. 1277-1284, 2020.
[http://dx.doi.org/10.1111/os.12740] [PMID: 32643308]

[15] J. Li, C. Xu, X. Zhang, Z. Xi, M. Liu, Z. Fang, N. Wang, L. Xie, and Y. Song, "TELD with limited foraminoplasty has potential biomechanical advantages over TELD with large annuloplasty: An in-silico study", *BMC Musculoskelet. Disord.,* vol. 22, no. 1, p. 616, 2021.
[http://dx.doi.org/10.1186/s12891-021-04504-1] [PMID: 34246272]

[16] W. Wu, R. Yu, H. Hao, K. Yang, G. Jiao, and H. Liu, "Visible trephine-based foraminoplasty in PTED leads to asymmetrical stress changes and instability in the surgical and adjacent segments: A finite element analysis", *J. Orthop. Surg. Res.,* vol. 18, no. 1, p. 431, 2023.
[http://dx.doi.org/10.1186/s13018-023-03916-0] [PMID: 37312161]

[17] X. Zhang, J. Lin, C. Liu, S. Xue, M. Wu, and Z. Yin, "Biomechanical changes in lumbar intervertebral discs after percutaneous endoscopic transforaminal discectomy surgery at different Body Mass Index (BMI) categories", *J. Orthop. Surg. Res.,* vol. 19, no. 1, p. 875, 2024.
[http://dx.doi.org/10.1186/s13018-024-05319-1] [PMID: 39726028]

[18] N.K. Singh, N.K. Singh, R. Verma, and A.D. Diwan, "Validation and estimation of obesity-induced intervertebral disc degeneration through subject-specific finite element modelling of functional spinal units", *Bioengineering,* vol. 11, no. 4, p. 344, 2024.
[http://dx.doi.org/10.3390/bioengineering11040344] [PMID: 38671766]

[19] M. Ahmadi, H. Chen, M. Lin, D. Biswas, J. Doulgeris, Y. Tang, E.D. Engeberg, J. Hashemi, G. Pires, and F.D. Vrionis, "Streamlined and efficient patient-specific modeling for lumbar spine segmentation and finite element analysis", *Sci. Rep.,* vol. 15, no. 1, p. 35619, 2025.
[http://dx.doi.org/10.1038/s41598-025-19664-6] [PMID: 41083563]

[20] M. Turbucz, A.J. Pokorni, G. Szőke, Z. Hoffer, R.M. Kiss, A. Lazary, and P.E. Eltes, "Development and validation of two intact lumbar spine finite element models for in silico investigations: Comparison of the bone modelling approaches", *Appl. Sci.,* vol. 12, no. 20, p. 10256, 2022.
[http://dx.doi.org/10.3390/app122010256]

[21] Z. Shi, L. Shi, X. Chen, J. Liu, H. Wu, C. Wang, Z. Chen, F. Yang, S. Yu, and Q. Pang, "The biomechanical effect on the adjacent L4/L5 segment of S1 superior facet arthroplasty: A finite element analysis for the male spine", *J. Orthop. Surg. Res.,* vol. 16, no. 1, p. 391, 2021.
[http://dx.doi.org/10.1186/s13018-021-02540-0] [PMID: 34140040]

[22] H.A. Wicaksono, L.J. Rama, M.I. Maula, I. Ammarullah, M.D.P. Lamura, A. Indra, P. Prasetya, and T.I. Winarni, "Analysis of von mises stress on lumbar 4 to sacral 1 with variation in body mass index", *J. Tribol.,* vol. 45, pp. 174-184, 2025.

[23] I. Yamamoto, M.M. Panjabi, T. Crisco, and T. Oxland, "Three-dimensional movements of the whole lumbar spine and lumbosacral joint", *Spine,* vol. 14, no. 11, pp. 1256-1260, 1989.
[http://dx.doi.org/10.1097/00007632-198911000-00020] [PMID: 2603060]

[24] W. Sun, D. Li, S. Zhao, H. Fu, J. Tian, F. Zhang, H. Feng, and D. Wu, "The effect of large channel-based foraminoplasty on lumbar biomechanics in percutaneous endoscopic discectomy: A finite element analysis", *J. Orthop. Surg. Res.,* vol. 19, no. 1, p. 402, 2024.
[http://dx.doi.org/10.1186/s13018-024-04870-1] [PMID: 38997769]

[25] S. Kang, C.H. Park, H. Jung, S. Lee, Y.S. Min, C.H. Kim, M. Cho, G.H. Jung, D.H. Kim, K.T. Kim, and J.M. Hwang, "Analysis of the physiological load on lumbar vertebrae in patients with osteoporosis: A finite-element study", *Sci. Rep.,* vol. 12, no. 1, p. 11001, 2022.
[http://dx.doi.org/10.1038/s41598-022-15241-3] [PMID: 35768481]

[26] B. Yang, and G.D. O'Connell, "Intervertebral disc swelling maintains strain homeostasis throughout the annulus fibrosus: A finite element analysis of healthy and degenerated discs", *Acta Biomater.,* vol. 100, pp. 61-74, 2019.
[http://dx.doi.org/10.1016/j.actbio.2019.09.035] [PMID: 31568880]

[27] C.P.L. Paul, M. de Graaf, A. Bisschop, R.M. Holewijn, P.M. van de Ven, B.J. van Royen, M.G. Mullender, T.H. Smit, and M.N. Helder, "Static axial overloading primes lumbar caprine intervertebral discs for posterior herniation", *PLoS One,* vol. 12, no. 4, p. e0174278, 2017.
[http://dx.doi.org/10.1371/journal.pone.0174278] [PMID: 28384266]

[28] J.C. Kienzler, P.D. Klassen, L.E. Miller, R. Assaker, V. Heidecke, S. Fröhlich, and C. Thomé, "Three-year results from a randomized trial of lumbar discectomy with annulus fibrosus occlusion in patients at high risk for reherniation", *Acta Neurochir.,* vol. 161, no. 7, pp. 1389-1396, 2019.
[http://dx.doi.org/10.1007/s00701-019-03948-8] [PMID: 31089894]

[29] F. Martens, P. Vajkoczy, S. Jadik, A. Hegewald, J. Stieber, and R. Hes, "Patients at the highest risk for reherniation following lumbar discectomy in a multicenter randomized controlled trial", *JBJS Open Access,* vol. 3, no. 2, p. e0037, 2018.

[http://dx.doi.org/10.2106/JBJS.OA.17.00037] [PMID: 30280130]

[30] M. Zhou, R.D. Huff, Y. Abubakr, and G.D. O'Connell, "Torque- and muscle-driven flexion induce disparate risks of in vitro herniation: A multiscale and multiphasic structure-based finite element study", *J. Biomech. Eng.,* vol. 144, no. 6, p. 061005, 2022. [http://dx.doi.org/10.1115/1.4053402] [PMID: 35079770]

[31] T.P. Green, M.A. Adams, and P. Dolan, "Tensile properties of the annulus fibrosus II. Ultimate tensile strength and fatigue life", *Eur. Spine J.*, vol. 2, no. 4, pp. 209-214, 1993. [http://dx.doi.org/10.1007/BF00299448] [PMID: 20058407]

[32] J.M. Middendorf, and V.H. Barocas, "An approach to quantify anisotropic multiaxial failure of the annulus fibrosus", *J. Biomech. Eng.,* vol. 146, no. 1, p. 014501, 2024. [http://dx.doi.org/10.1115/1.4063822] [PMID: 37851527]

[33] D.S. Meredith, R.C. Huang, J. Nguyen, and S. Lyman, "Obesity increases the risk of recurrent herniated nucleus pulposus after lumbar microdiscectomy", *Spine J.,* vol. 10, no. 7, pp. 575-580, 2010. [http://dx.doi.org/10.1016/j.spinee.2010.02.021] [PMID: 20347400]

[34] K. Nakajima, J. Miyahara, N. Ohtomo, K. Nagata, S. Kato, T. Doi, Y. Matsubayashi, Y. Taniguchi, N. Kawamura, A. Higashikawa, Y. Takeshita, M. Fukushima, T. Ono, N. Hara, S. Azuma, H. Iwai, M. Oshina, S. Sugita, S. Hirai, K. Masuda, S. Tanaka, and Y. Oshima, "Impact of body mass index on outcomes after lumbar spine surgery", *Sci. Rep.,* vol. 13, no. 1, p. 7862, 2023. [http://dx.doi.org/10.1038/s41598-023-35008-8] [PMID: 37188788]

[35] T. Herold, R. Kothe, C.J. Siepe, O. Heese, W. Hitzl, A. Korge, and K. Wuertz-Kozak, "Effect of BMI on the clinical outcome following microsurgical decompression in over-the-top technique: Bi-centric study with an analysis of 744 patients", *Eur. Spine J.,* vol. 30, no. 4, pp. 936-945, 2021. [http://dx.doi.org/10.1007/s00586-021-06765-9] [PMID: 33638720]

[36] A. Abdi, S.R. Bagheri, Z. Shekarbeigi, S. Usefvand, and E. Alimohammadi, "The effect of repeated flexion-based exercises versus extension-based exercises on the clinical outcomes of patients with lumbar disk herniation surgery: A randomized clinical trial", *Neurol. Res.,* vol. 45, no. 1, pp. 28-40, 2023. [http://dx.doi.org/10.1080/01616412.2022.2116686] [PMID: 36039973]

[37] C.H. Park, J. Beom, C.K. Chung, C.H. Kim, M.Y. Lee, M.W. Park, K. Kim, and S.G. Chung, "Long-term effects of lumbar flexion versus extension exercises for chronic axial low back pain: A randomized controlled trial", *Sci. Rep.,* vol. 14, no. 1, p. 2714, 2024. [http://dx.doi.org/10.1038/s41598-024-51769-2] [PMID: 38302483]

[38] W. Golonka, C. Raschka, V.M. Harandi, B. Domokos, H. Alfredson, F.M. Alfen, and C. Spang, "Isolated lumbar extension resistance exercise in limited range of motion for patients with lumbar radiculopathy and disk herniation—clinical outcome and influencing factors", *J. Clin. Med.,* vol. 10, no. 11, p. 2430, 2021. [http://dx.doi.org/10.3390/jcm10112430] [PMID: 34070780]

[39] V. Abdollah, E.C. Parent, and M.C. Battié, "MRI evaluation of the effects of extension exercises on the disc fluid content and location of the centroid of the fluid distribution", *Musculoskelet. Sci. Pract.,* vol. 33, pp. 67-70, 2018. [http://dx.doi.org/10.1016/j.msksp.2017.11.008] [PMID: 29180112]

[40] Y. Zhu, S. Xia, W. Yang, F. Shi, and H. Ji, "Early efficacy of postoperative rehabilitation training for lumbar disc herniation", *BMC Sports Sci. Med. Rehabil.,* vol. 15, no. 1, p. 97, 2023. [http://dx.doi.org/10.1186/s13102-023-00704-5] [PMID: 37553676]